Unveiling the beauty of darkened soda-lime glass through infrared femtosecond laser processing

Nikolay Busleev[1] · Nikita Smirnov[1] · Vladimir Kesaev[1] · Sergey Kudryashov[1]

Abstract

This research work focuses on investigating the darkening phenomenon in soda-lime glasses caused by the formation of color centers when exposed to infrared femtosecond laser radiation. The study examines the kinetics of color center generation and thermal relaxation, with a particular emphasis on the influence of storage temperature. Additionally, the changes in transmittance and refractive index values of darkened glass were measured based on different laser processing parameters. The darkening process can be utilized for the creation of halftone monochrome images for decorative purposes. The study also discusses the achievable contrast values and their degradation over time. Our findings were supported by direct laser writing of an image into the glass volume, highlighting their practical interest.

1 Introduction

Ultrafast lasers are widely used for changing optical properties and structuring of transparent dielectrics, such as glasses. Parameters of laser radiation strongly affect the outcome of laser–matter interaction, which can include an increase of refractive index as a result of the densification [1], creation of birefringent structures [2], or the formation of voids [3]. It also has been shown that interaction of ultrafast laser pulses with common soda-lime glass can produce coloration [4–6], which is caused by the accumulation of color centers in the irradiated volume [7, 8].

The process of creating darkened tracks within soda-lime glass through the use of femtosecond laser pulses is achieved by focusing the pulses with energy above a threshold into the glass volume. This leads to a visible loss of transparency and a noticeable darkening that can be observed with the naked eye. Geometrical dimensions of these tracks, its length, and radius depend on parameters of the optical system. These values can be varied from several microns to dozens of millimeters, which is considerably exceeding the spacial length of the femtosecond laser pulse. The total number of pulses per unit volume, rather than pulse energy value, plays a critical role in laser processing of glass. Ultimately, there is a limit value of darkening that can be asymptotically achieved by increasing the overall energy delivered to the material—exposure.

It should be noted that the described effect is temporally unstable, as the relaxation process begins after femtosecond laser processing, which gradually decreases the darkening magnitude and restores transparency over time. The relaxation process is influenced by external factors such as temperature and exposure to low-energy blue and UV electromagnetic radiation. Relaxation, also known as bleaching, has an asymptotic character, tending towards a residual level without completely restoring the original glass transparency. Both darkening and bleaching kinetics are Markov processes, meaning that their evolution depends only on the current state and not on previous states.

The darkening of glasses, produced by X-ray [9–12] or UV radiation [13, 14], is well known. However, the nature of this effect is currently not completely clear; in most studies, it is associated with the formation of various defects. Color centers responsible for the brownish color of the glass are classified as non-bridging oxygen hole centers (NBOHCs). The released electrons from NBOs are trapped at glass-modifying (alkaline and alkaline earth) ions and dopant cations. The reverse reaction is the return of trapped electrons to NBOHCs through photo- or thermally activated processes.

✉ Nikolay Busleev
  busleevni@lebedev.ru

1 P. N. Lebedev Physical Institute of the Russian Academy of Sciences, Moscow, Russia

2 Theory

In our experiments, we observe that different types of glass exhibit distinct modifications after processing with femtosecond laser pulses. For instance, uranium glass loses its luminescence under UV radiation, while chalcogenide glass exhibits red spectral luminescence under green radiation. Brown-colored glasses containing iron oxide pigments (common in the food and pharmaceutical industries) show an increase in transparency after femtosecond laser processing, contrary to the expected darkening effect. The magnitude of these changes in glass properties decreases over time, and the original material behavior is gradually restored. It seems that the chemical composition of the glass and its manufacturing process are crucial factors influencing the observed color centers, darkening magnitude, and temporal stability. Some soda-lime glass samples bleach rapidly within minutes, while others remain darkened for months.

We studied the kinetics of color centers generation depending on number of laser pulses and pulse energy. Thus, our main interest is color centers concentration in volume $C(H)$ depending on exposure H which is generally delivered to the material non-instantly. We also analyze the kinetics of relaxation which occurs at different rates depending on temperature and glass composition. The concentration C convenient to evaluate through optical density D, which can be easily measured in experiment. Optical density D is directly proportional to color centers concentration in volume [15],

$$D = \alpha C z = -lg(T), \tag{1}$$

where α—absorption cross section $[L^2]$, z—sample thickness and T—transmittance. Since $C \bullet z$ dimensions are $[L^{-3} \bullet L] = [L^{-2}]$, therefore D and T are dimensionless values. Optical density is not only useful for analysis convenience but also represents practical interest. We will discuss the high-resolution writing of halftone monochromatic images inside the glass volume as an example further in the article.

Color centers concentration in volume is typically described by "stretched exponential" Kohlrausch function [16]:

$$C(H) = C_c(kH)^\beta + C_a\{1 - exp[-(k\dot{H}t)^\beta]\}, k = k_a + k_d, 0 \le \beta \le 1, \tag{2}$$

that only includes exposure H and exposure rate $\frac{dH}{dt}$ as controlled experimental values. For the case of an ultrafast laser, these quantities require an explanation, given below in the text. It should be noted, that H is a total radiation energy, delivered to the unit volume of the material. The concentrations, which are included in Eq. (2)'

$$C_c = \left(\frac{k_c}{k}\right)^\beta \frac{k_a}{k_0}, C_a = \left(\frac{k_c}{k}\right)^\beta \frac{k_d}{k_0} + \frac{k_a}{k_p}(0) \tag{3}$$

depend on material constants $\{k_a, k_c, k_d\}$. These constants characterize the relationship with the lower limit concentrations of color centers C_0 and precursors C_p. Such system corresponds to the diagram:

$$C_0 \to^{k_c} C \underset{k_d}{\overset{k_a}{\rightleftarrows}} C_p. \tag{4}$$

Under the effect of laser radiation, part of possible color centers are activated $C_0 \overset{k_c}{\to} C$ proportionately to k_c. Precursors, the nature of which is associated with neutral oxygen vacancies in glassy SiO_2, make competing contributions to the activation $C_p \overset{k_a}{\to} C$ and, at the same time, deactivation $C \overset{k_d}{\to} C_p$.

Kinetics described by Kohlrausch function (2) can be obtained by solving an equation of the form $d\phi/dt = -\eta\phi$, with a change of variable $t \to t^b$ and constant $\eta \to \eta^b, 0 \le b \le 1$ [16, 17]. In this case, the kinetics will be described by the equation $d\phi/d(t^b) = -\eta^b\phi$, and the solution will be $\phi = exp\{-(\eta t)^b\}$. Here, non-integer exponent $0 \le b \le 1$ translates the dimensions of the Euclidean space into the so-called fractal dimensions.

As a starting point, we will redefine concentrations $C_{a,c}$ and adapt Eq. (2) for practical convenience. Figure 1a shows the experimentally observed color centers concentration growth kinetics. The exposure is shown on the x-axis and defined as a number of pulses n with the energy E_0, equal to energy value of single laser pulse that generates irreversible color centers concentration C_0:

$$H = nE_0. \tag{5}$$

The horizontal line to which the concentration tends during the process of relaxation after laser processing corresponds to irreversible aftereffect color centers concentration C_0. Let us assume that concentrations below
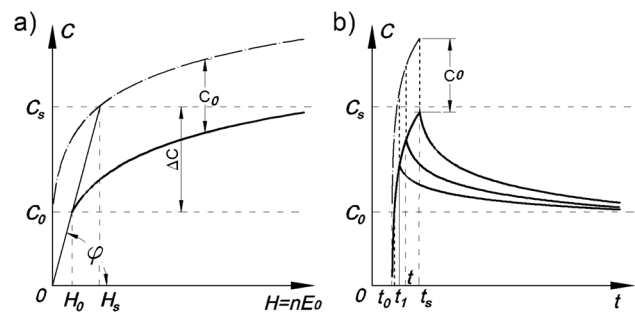
Fig. 1 **a** Kinetics of color centers concentration C growth depending on exposure H. **b** Kinetics of color centers concentration C relaxation depending on time t

C_0 are instantaneously and completely reversible after the termination of laser processing at times unresolvable in our experiment. Here, instantaneous times are times of the order of $10^{-9} \div 10^{-6}$, which characterize the lifetime of the excited state of the atom.

It is important to emphasize that C_0 does not mean the concentration corresponding to the threshold energy of the laser pulse at which a colored track appears, but the equilibrium value of concentration during relaxation. Exposure H_0 in practice does not coincide with the real energy of a single pulse, at which darkening appears. On the contrary, according to (5), for the concentration C_0 we correspond the exposure $H_0 = E_0$ of a conditional single pulse ($n = 1$). Such simplification is acceptable for our case, since in our experiments the pulse repetition rate was relatively small $f \sim 10^4$ Hz.

Oblique line, drawn from zero to the point of intersection with a line C_0 corresponds to a linear increase in concentration, directly proportional to $K = \frac{dC}{dH} = tan\varphi$. Taking this into account, we can assume that the concentration $C \leq C_0$ depends linearly on H. Horizontal line C_s (saturated concentration) corresponds to the upper limit color centers concentration, to which concentration C asymptotically tends in case of unlimited exposure H. Both quantities C_0 and C_s characterize the properties of the material.

Now, we rewrite (2) taking into account the new definitions of concentrations and under the condition of a constant pulse repetition rate ($\dot{H}t = const$):

$$C(H) = KH_0 + \Delta C\{1 - exp[-(kH)^\beta]\}, \tag{6}$$

where $\Delta C \equiv C_s - C_0 = K(E_s - E_0)$, and $KH_0 = C_0$. Now, we can characterize glass by a set of four parameters, C_s, C_0, k, and β, two of which, C_s и C_0, can be directly measured, and the remaining two, k and β can be easily obtained by fitting the concentration (darkening) curve using the Eq. (6).

The assumption of a concentration with an instantaneous relaxation is equivalent to an upward shift for the observed concentration growth curve by C_0, as shown on Fig. 1a. After laser processing the relaxation occurs, consisting of two stages, instantaneous relaxation by the value of C_0 and subsequent long-term relaxation. Figure 1b shows the growth curve in the time period $t_0 \div t_s$ and the relaxation curves for the cases when laser irradiation stops at the time points $t_0 \leq t \leq t_s$. All of them tend to the C_0 level. As we will see below, the relaxation kinetics is also described by an equation similar to (6) with a change of variables $KH_0 \to C_s$, $(kH)^\beta \to (\zeta t)^\beta$ and the sign before the second term,

$$C(H) = C_s - \Delta C\{1 - exp[-(\zeta t)^\beta]\}. \tag{7}$$

Thus, relaxation is characterized by four parameters C_s, C_0, ζ and β, three of which coincide with the parameters used to describe the concentration growth kinetics as a function of H.

The decrement $log\{\zeta(\Delta T)\}$ turns out to be strongly linearly dependent on the temperature T,

$$log\left(\frac{\zeta(\Delta T)}{\zeta_{21}}\right) = \chi\Delta T, \tag{8}$$

where ζ_{21}—the decrement at room temperature 21 $^{\circ}$C; χ—the proportionality factor, and $\Delta T = T - 21$—difference between current sample temperature T and room temperature.

The equations obtained in this study can be utilized for controlling the darkening process of soda-lime glass. The optical density of samples processed through multiple procedures was examined to determine its dependence. Despite the intense relaxation processes that occur within the first few minutes, the optical density demonstrates additivity, which facilitates the use of existing galvo scanners software. To create decorative images, dividing the original image into numerous grayscale ranges is sufficient for producing a halftone image in glass. Additionally, digital image processing techniques such as Floyd–Steinberg dithering can be employed and increasing the number of ranges may further improve the halftone reproduction. The achieved halftone reproduction was good in all cases, with technological factors being the only limitation.

3 Experimental details and analysis methods

The experimental setup is shown in Fig. 2a. A TETA-20 (Avesta) femtosecond laser system with a maximum power of up to 20 W and a pulse repetition rate of up to 200 kHz was used as a source of laser radiation. The glass was processed using a central wavelength of 1030 nm and a pulse duration of 250 fs. A collimated beam with a diameter of 4 mm, exiting the laser system, was directed into a galvo scanner using dielectric mirrors. Galvo scanner was equipped with a F-theta lens with a focal length of 100 mm which made it possible to focus the beam into a spot with a diameter of about $2\omega_0 = 26$ μm with a Gaussian intensity distribution. The working field of the galvo scanner was 70×70 mm. We should note here that only a part of the delivered energy is involved in glass modification thus the diameter of the area with laser intensity above the darkening threshold $2\omega\prime_0$, depending on the threshold value for each glass, was smaller. The focal plane of the F-theta lens was always located on the lower surface of the glass sample with a depth of $z = \delta$ (Fig. 2d). The scanning was carried out line by line with independent and quasi-linear scanning speeds in two orthogonal directions XY, the
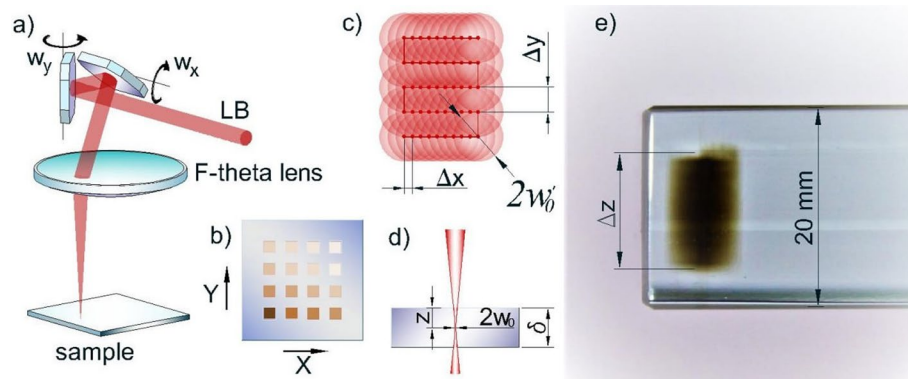
Fig. 2 Scheme of 2D modification of glass by femtosecond laser radiation. **a** Scanning a two-dimensional image in glass using a galvo scanner. **b** An example of set of images where the pulse energy was changed along the x-axis and the scanning speed was changed along the y-axis. **c** Scheme of two-dimensional scanning of laser radiation in the XY plane. **d** Scheme of focusing laser radiation into the sample. **e** The photo of the modified region in the sample taken from the side (perpendicular to the laser beam propagation direction) to determine the threshold energy values and the diameter $2\omega'_0$ of the area with laser intensity above the darkening threshold

Table 1 Chemical composition of soda-lime glass samples

Element	Sample 1 Atomic %	Sample 2 Atomic %	Sample 3 Atomic %
O	63.69	60.74	59.73
Si	25.41	24.48	25.41
Na	7.38	9.35	8.66
K	2.99	0.15	0.11
Ca	0	2.51	3.16
Mg	0	2.16	1.86
Ba	0.41	0	0
Sn	0	0	0.70
Al	0	0.51	0.34
As	0.08	0	0
Cl	0.04	0	0
Fe	0	0	0.04
S	0	0.09	0

angular velocities of the horizontal (W_x) and vertical (W_y) mirrors were controlled independently. A substrate with soda-lime glass samples was located under the lens. The samples, which are glass plates with polished upper and lower surfaces $1 \leq \delta \leq 20$ mm thick, were always motionless during processing.

As will be shown later, $2\omega'_0$ can be found by analyzing Fig. 2e showing a 5×5 mm modified region in thick glass ($\delta = 20$ mm). The photo was taken from the side, thus showing the modification along the length of the waist (along the z axis); its length for the glass used was 11 mm. In this case, the focus was located at the bottom of the modified region.

The chemical composition of each of the soda-lime glass samples was obtained on an Xplore EDS detector (Oxford Instruments) and is presented in Table 1. The thickness of samples ranged from 1 to 3 mm.

Glass modification was carried out at different values of the pulse energy and the number of pulses per unit area. The laser pulse energy was gradually varied using a laser radiation attenuator based on a half-wave plate and a polarizer built into the laser system. The repetition rate of laser pulses was constant (10 kHz), and the number of pulses per unit area was varied by changing the scanning speed of the laser beam. The pulse energy was varied from 10 to 40 µJ and the scanning speed—from 5 to 1000 mm/s. In each sample, areas ranging in size from 4×4 to 10×10 mm were recorded and a color change was observed throughout the entire thickness of the samples (1–3 mm). The shape and size of the processed area were set in the galvo scanner software. The filling of the areas was bi-directional with a line spacing of 3 µm. The substrate was moved along the z-axis with a minimum step of 2.5 µm. To prevent ablation of the upper surface of the glass upon reaching high energy values, the height of the substrate was adjusted so that the focus of the F-theta lens was located at the lower edge of the sample.

After laser processing, coloration of glass samples was observed. Various magnitudes of darkening depend on such parameters as pulse energy and scanning velocity. The refractive index change, white light transmittance and thermal stability of modified regions were measured.

Small changes in the refractive index of the modified glass were measured in two ways: the prism method and the interferometric method. In the first method, a sample was made with four plane-parallel polished faces (Sample 1). A triangular prism 5×5 mm was formed in the volume of the sample by laser radiation as shown in Fig. 3a. Then, the sample with a prism was placed in a low-power undivided beam of a helium–neon laser ($\lambda = 632.8$ nm) and shifted in such a way that the beam first passed through clean glass and then through the prism (the corresponding beam scheme is shown in Fig. 3a). In the experiment two cases were compared:
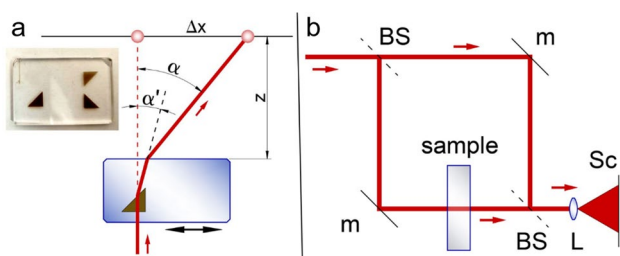
Fig. 3 a Setup for measuring the refractive index change by the prism method. The distance z to the screen was 6 m; the thickness of the sample was 3 mm. **b** Setup for measuring the refractive index change by the interferometric method. BS—beam splitter, m—mirror, L—lens, Sc—screen

Fig. 4 a Sample with regions processed at different energies and scanning speeds. **b** The resulting interferogram obtained by a Mach–Zehnder interferometer. Sample 1 was used

laser beam passing through the sample area with and without the prism. The displacement Δx of the light spot for the case of the prism relatively to the initial position without the prism was measured on a screen remoted at a distance z.

The first method succeeded in establishing the value of the refractive index increment only for the darkest prism. It amounted to $4.2 \cdot 10^{-5} \pm 5 \cdot 10^{-6}$ for a total exposure of $\sim 2.4 \cdot 10^3$ µJ/µm². In addition, by the direction of beam deflection, this method made it possible to reliably establish the sign of the refractive index change (RIC) which turned out to be positive. Since the deflection angles for small RICs were comparable with the diffraction divergence of the laser, further measurements were performed using the interferometric method.

To determine the RIC by the interferometric method, we built a two-beam Mach–Zehnder interferometer. A collimated light beam with a diameter of about 3.8 cm from a helium–neon laser was directed at the input of the interferometer. A sample was then placed in one of the arms along the normal to the passing beam, as illustrated in Fig. 3b. The interferometer was tuned in fringes of finite thickness to facilitate analysis of the output interferogram. Examples of a sample and an interferogram obtained from it are shown in Fig. 4. The interferograms displayed a relatively wide transition zone between the modified and unmodified glass without breaking of interferometric fringes, enabling us to reliably establish the order of interference. Meanwhile, the sign of the RIC was established using the previous prism method. The increment of the refractive index Δn was calculated by the following formula:

$$\Delta n = \frac{\Delta x}{P} \frac{\lambda}{2} \frac{1}{t}, \tag{9}$$

where Δx—shift of the interference maximum (minimum) in the modified area of the sample relative to unmodified glass, P—interference pattern period, t—sample thickness.

White light transmittance of every modified glass region was measured by photoelectric power meter
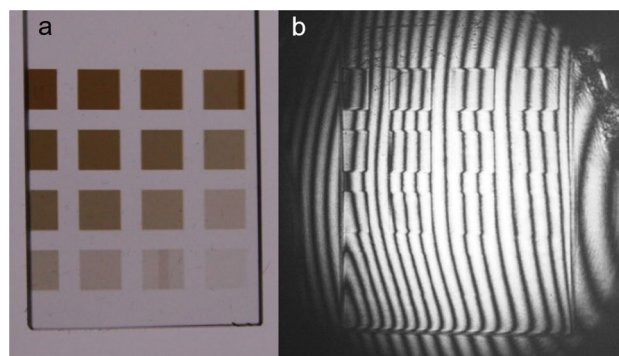
Liconix 45PM and LED light bulb with the color temperature 4000 K and power 8W.

Sample 2 was also processed and the modified regions were characterized using optical spectroscopy after various periods of time, while each sample was stored at different temperature conditions: at room temperature ($+ 21$ °C), in a freezer ($- 21$ °C) and in a heated oven with a PID controller ($+ 100$ °C). The measurements were carried out using a SF-2000 spectrophotometer (OKB Spectr).

The absorbance of the modified glass region is shown in Fig. 5a and was calculated as follows. First, two identical glass samples with a thickness of 1 mm were taken and regions of 10×10 mm were modified in each of them at a pulse energy of 40 µJ and a scanning speed of 50 mm/s. Immediately after the processing, the transmittance spectra of the modified region were measured for two cases: one sample and two samples stacked together. The αC value was calculated using the Beer–Lambert law:

$$\frac{I_1}{I_2} = \frac{I_0}{I_0} \frac{e^{-\alpha C z_1}}{e^{-\alpha C z_2}} = e^{-\alpha C \Delta z}, \alpha C = -\frac{1}{\Delta z} \ln \frac{I_1}{I_2}, \tag{10}$$

where z_1 and z_2—thicknesses of one and two samples, respectively, I_1 and I_2—the light intensities passing through one and two modified glass regions. From the values of αC, the transmittance spectrum was calculated for one sample with a thickness of 1 mm. The normalized intensity of Rayleigh scattering, which is inversely proportional to the fourth power of the wavelength ($I_R = \frac{R}{\lambda^4}$, where R—the proportionality factor) is shown in Fig. 5b. By subtracting the transmittance spectrum from the theoretical curve, the absorbance spectrum can be obtained. The characteristic peaks in Fig. 5a around 450 and 630 nm refer to induced NBOHCs type color centers that are responsible for the observed brown tint of the processed regions [12, 13].
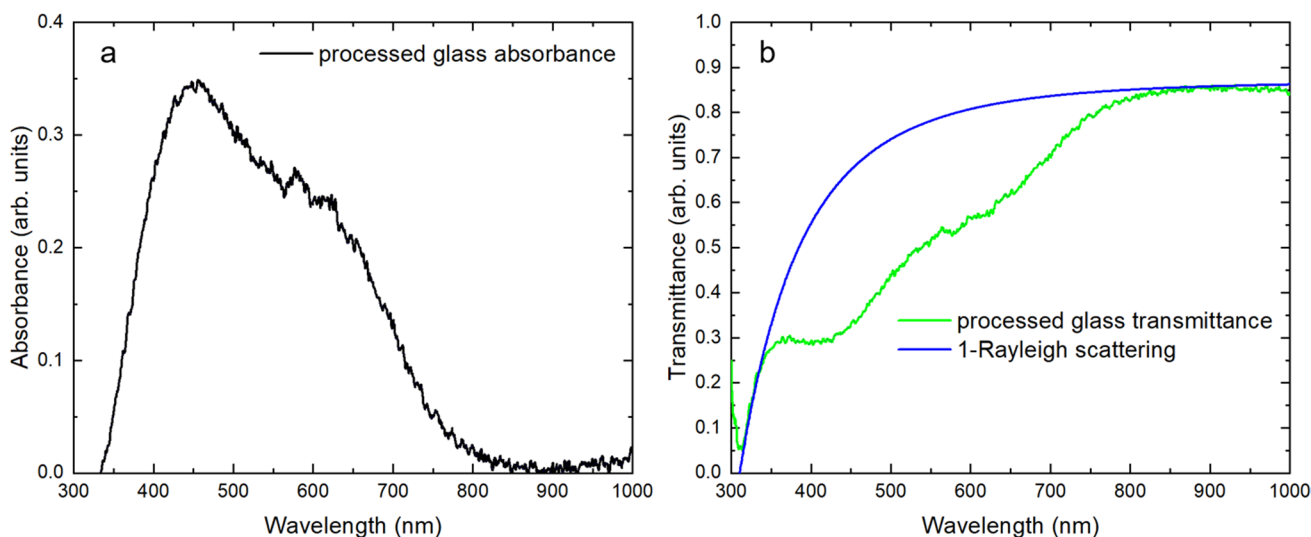
Fig. 5 Calculated spectra of **a** absorbance and **b** transmittance and Rayleigh scattering of the modified glass with a thickness of 1 mm. Sample 2 was used

4 Results and discussion

Changes of the refractive index and white light transmittance of modified regions depending on the pulse energy and scanning speed are shown on graphs in Fig. 6. Values were measured for each of the 16 square modified regions (shown in Fig. 4) and then interpolated to create a 3D surface. From the first graph, it can be seen that RIC is more strongly dependent on the pulse energy, while as the scan speed increases, RIC reaches a plateau. The second graph shows that the white light transmittance falls off much faster with decreasing scanning speed than with increasing energy.

Graphs of RIC and optical density depending on the exposure are shown in Fig. 7. Exposure values were calculated from pulse energy and scanning speed values for each of 16 regions. It can be seen from Fig. 7a that the change in the refractive index depends non-monotonically on the exposure, while as the exposure increases, the optical density reaches the maximum level according to Eq. (6). As shown in Fig. 7c, refractive index change is strongly affected by pulse energy value, while the influence of scanning speed is weaker. It should be additionally noted that after heating the sample in the oven the magnitude of darkening lowers significantly while RIC value remains unchanged.

For modified regions created at a pulse energy of 40 μJ and a scanning speed of 50 mm/s, optical density values
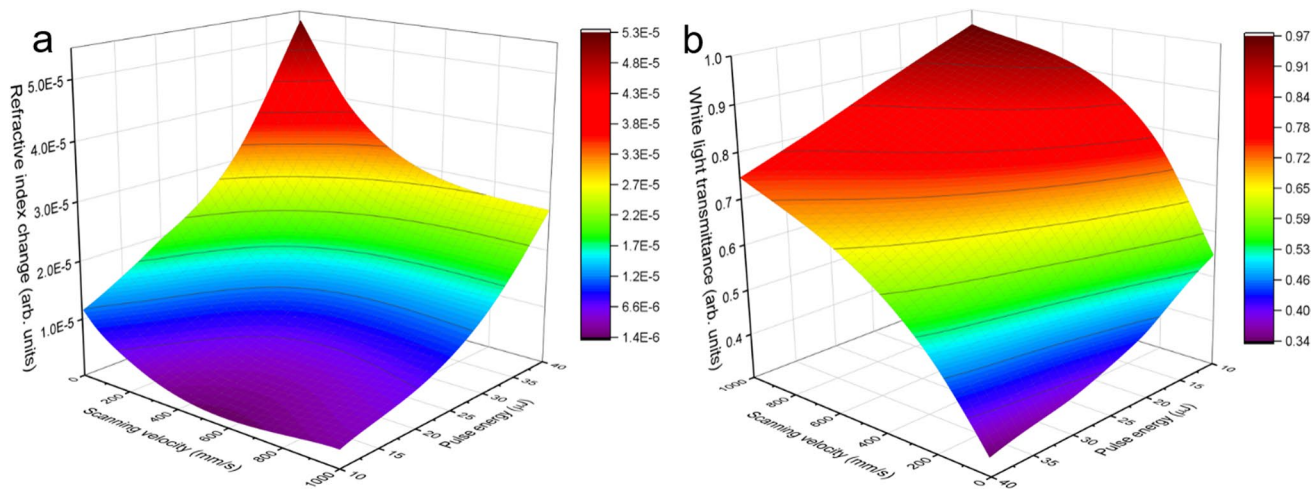
Fig. 6 **a** Refractive index change and **b** white light transmittance depending on the pulse energy and scanning speed. Sample 1 was used
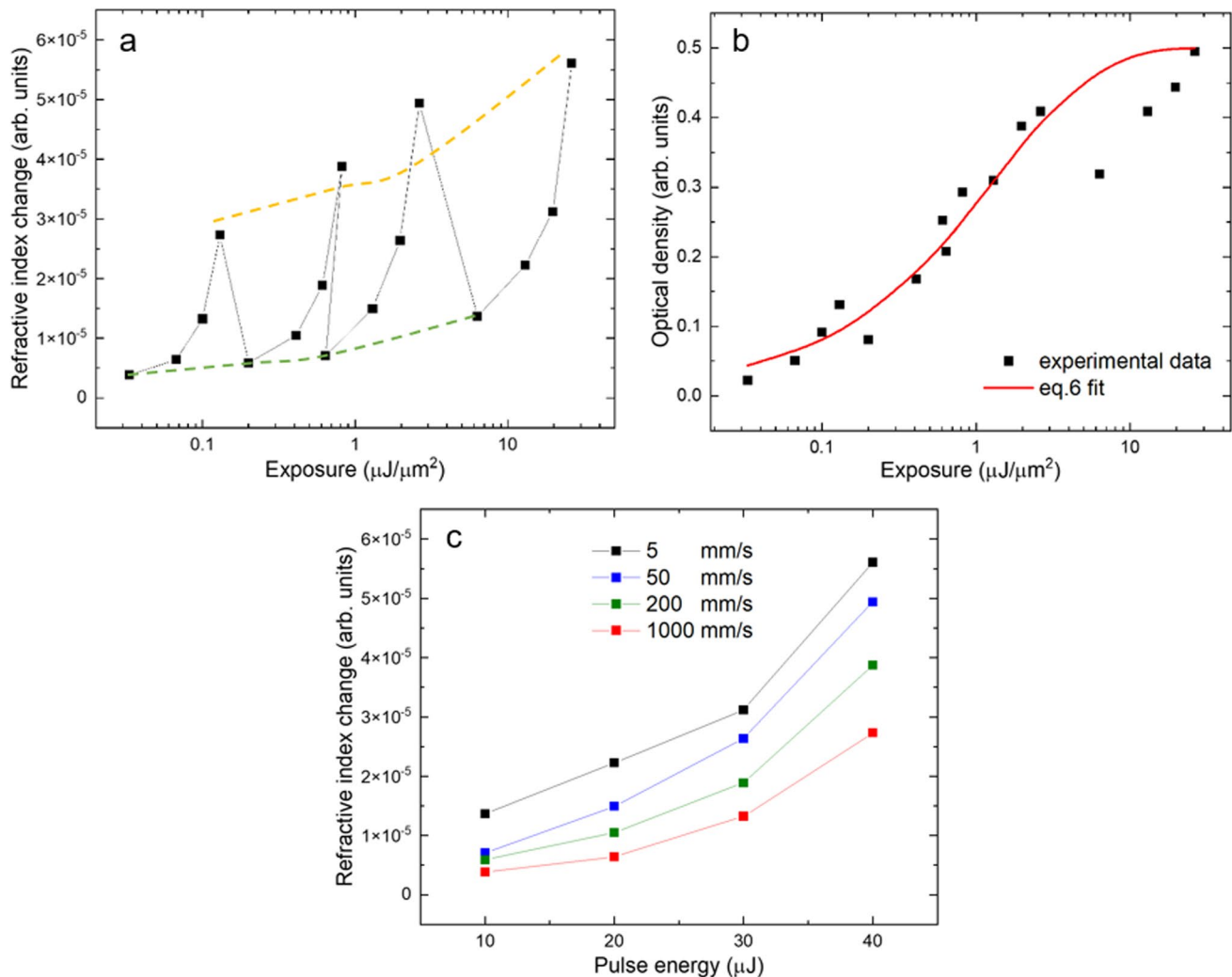
Fig. 7 **a** Refractive index change and **b** optical density depending on the exposure. Sample 1 was used. Green dash line connects experimental data with pulse energy 10 µJ and various scanning speed. Yellow dash line—40 µJ and various scanning speed. **c** Refractive index change depending on the pulse energy for each scanning speed value

were measured as a function of time after glass modification and sample storage temperature (Fig. 8). The processed regions have low thermal stability, similar to the color centers obtained in soda-lime glass using X-ray [9].

The additivity of optical densities of the successively processed glass was studied on Sample 3 (Fig. 9). Six 4×4 mm areas were processed, each of which received 1–6 laser processing procedures (Fig. 9b inset). The exposure remained unchanged for each processing procedure (40 µJ, 200 mm/s). Immediately after this, white light transmittance was measured for each section. The first graph (Fig. 9a) shows the approach of optical density with each subsequent processing to the saturation level according to Eq. 6.

Using Eq. 6, characteristic curves were plotted for sample 1 and 3 (Fig. 10a), using the coefficient values determined by fitting the experimental data. Knowing the straight

section of the characteristic curve of the photosensitive material, it is possible to calculate the exposure latitude described by the expression $L = log\frac{H_2}{H_1}$. In our case, $L_1 \sim 0.59$ and $L_3 \sim 1$. This value determines the allowable brightness range of the written image.

The contrast is defined as $\gamma = \Delta D / \Delta log(H)$, i.e., as the tangent of the angle of the straight section of the characteristic curve to the abscissa axis. Curves in Fig. 9a can be viewed as such straight sections for sample 3. As can be seen from the curve in Fig. 9a, corresponding to the time 8434 min, this angle decreased significantly, which corresponds to a decrease in the contrast value for modified areas with different number of procedures (Fig. 9b). Since, according to Eq. 1, optical density is directly proportional to the thickness of the sample, in theory the contrast can be
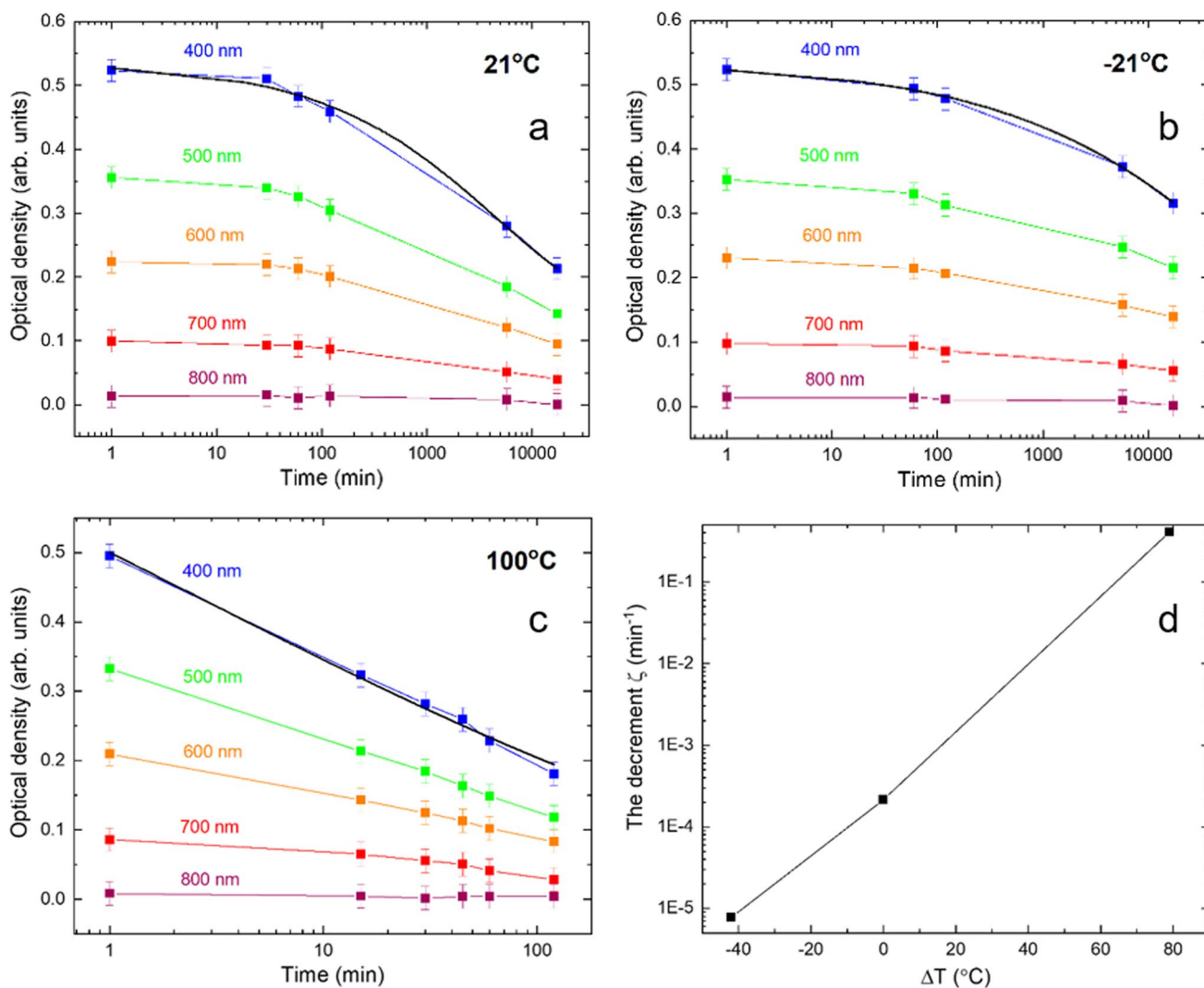
Fig. 8 Optical density depending on time after glass modification and sample storage temperature. The sample was stored in: **a** room at 21 °C; **b** freezer at -21 °C; **c** oven at 100 °C. Laser processing parameters used: pulse energy 40 µJ, scanning speed 50 mm/s. Black curve—Eq. 7 fit. Sample 2 was used. **d** The decrement $\zeta(T)$, calculated from Eq. 7 fit

increased using thicker samples. For sample 3 with double and triple thickness, the contrast value will be $\gamma_{3double} \sim 0.44$ and $\gamma_{3triple} \sim 0.66$. Contrast for sample 1 calculated from the characteristic curve in Fig. 10a is equal to $\gamma_1 \sim 0.29$.

Obtaining black and white halftones is shown in Fig. 10b. A continuous black and white gradient was used as the original image. To obtain a discrete set of halftones in glass, this image was divided into the required number of layers with the same grayscale step. Dither was additionally used in the software of the galvo scanner to obtain a continuous gradient.

To measure the maximum resolution of the written image, which can be achieved on a conventional commercial galvo scanner, a resolution test chart was written in the sample 3 (Fig. 11a). The dimensions of resolution test chart were 25×18.6 mm, the pulse energy used was 2.5 µJ and scanning speed was 25 mm/s. The last group has pronounced image defects, however, the distinguishable elements allow us to estimate the maximum writing resolution of ~ 10µm.

To estimate the exposure value in our experiments, we calculated the diameter $2\omega'_0$ of the area with laser intensity above the darkening threshold within which the glass is modified. First, the glass modification height along the z-axis was measured for a pulse energy of 100µJ written in thick glass (Fig. 2e). During processing the focus was located in the lower plane of the darkened region. The intensity of laser radiation after normalization is described by the expression $I \sim e^{-2(r^2/\omega(z)^2)}$, where: $r^2 = x^2 + y^2$—the radial coordinate, $\omega(z) = \omega_0 \sqrt{1 + \left(\lambda z / \pi n \omega_0^2\right)^2}$—the waist radius, z—the coordinate along the beam measured from the focus and $n = 1.5113$—medium refractive index [18].
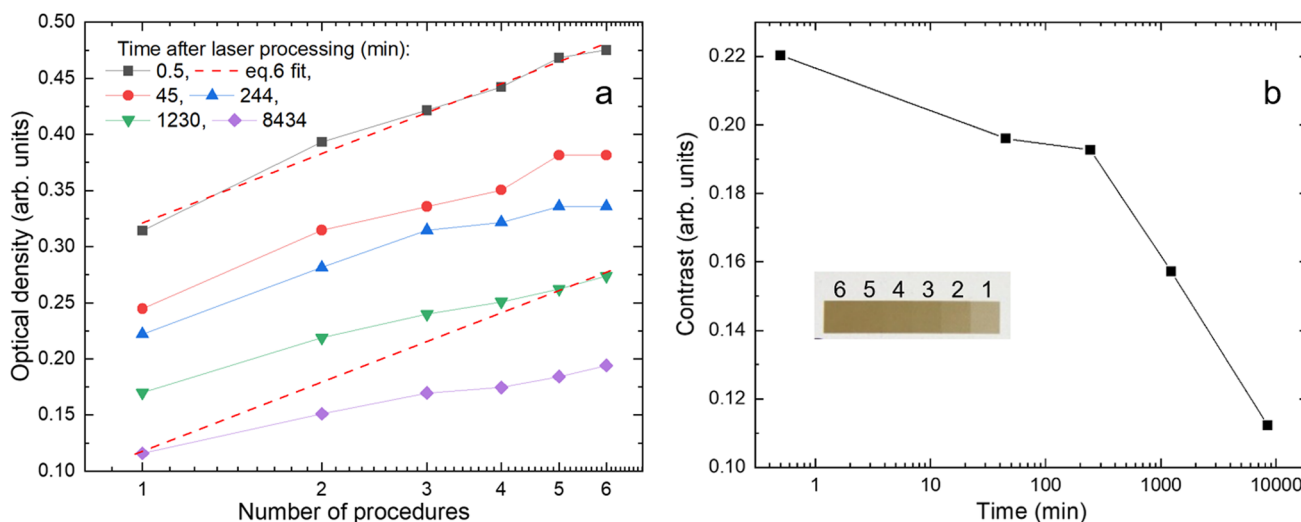
Fig. 9 a Optical density of each area received from 1 to 6 successive processing procedures depending on time. Lower red dash line is a copy of Eq. 6 fit added to show the decrease of angle between curves and x-axis with time. **b** Contrast of six areas depending on time. Insert: photo of modified areas with the indicated number of procedures. Sample 3 was used
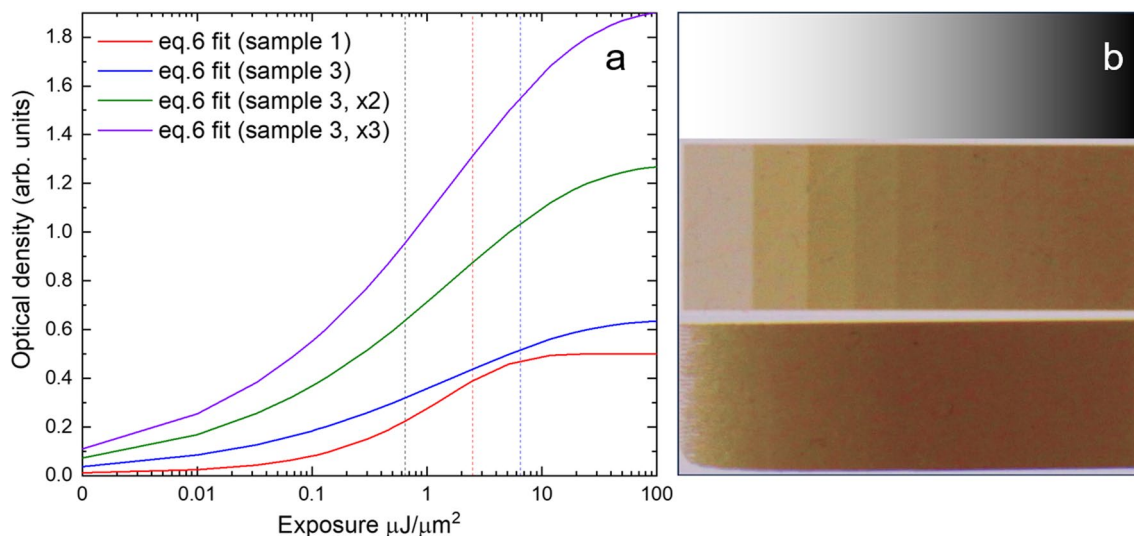

Fig. 10 a Calculated characteristic curves for samples 1, 3 and sample 3 with double and triple thickness (6 and 9 mm, respectively). Dashed lines show straight sections of characteristic curves: black— red for sample 1 and black—blue for sample 3. **b** From top to bottom: original image of continuous black and white gradient, discrete gradient and continuous gradient written in glass

The quality factor of our laser beam is $M^2 \leq 1.2$, and its diameter is $D \approx 4$ mm, therefore the diffraction-limited size of the spot focused by F-theta lens was $2w_0 = \frac{4M^2 \lambda f}{\pi D n} \approx 26$ μm. As mentioned above, laser radiation with $\lambda = 1030$ nm was used and focal length of our F-theta lens was 100 mm.

Considering the equation for the waist radius $\omega(z)$, the intensity in the upper plane of the darkened region $I_{xy}(z)$ was calculated, which is the lowest value of the intensity at which darkening occurs. Using the ratio of the intensities at the beam center for the z values in the upper plane and at the focus position ($I_{00}(z)$ and $I_{00}(0)$), the radius $\omega_0\prime$ was calculated, within which the $I_{xy}(0)$ exceeds the value required for glass modification. The part of the intensity profile lying within this radius was considered to be contributing to the darkening process. In our experiments, except for the case of a scanning speed of 1000 mm/s, the steps Δx and Δy did not exceed $2\omega_0\prime$ which is $78\% \div 22\%$ of $2\omega_0$. Thus, the exposure in our case is calculated as the
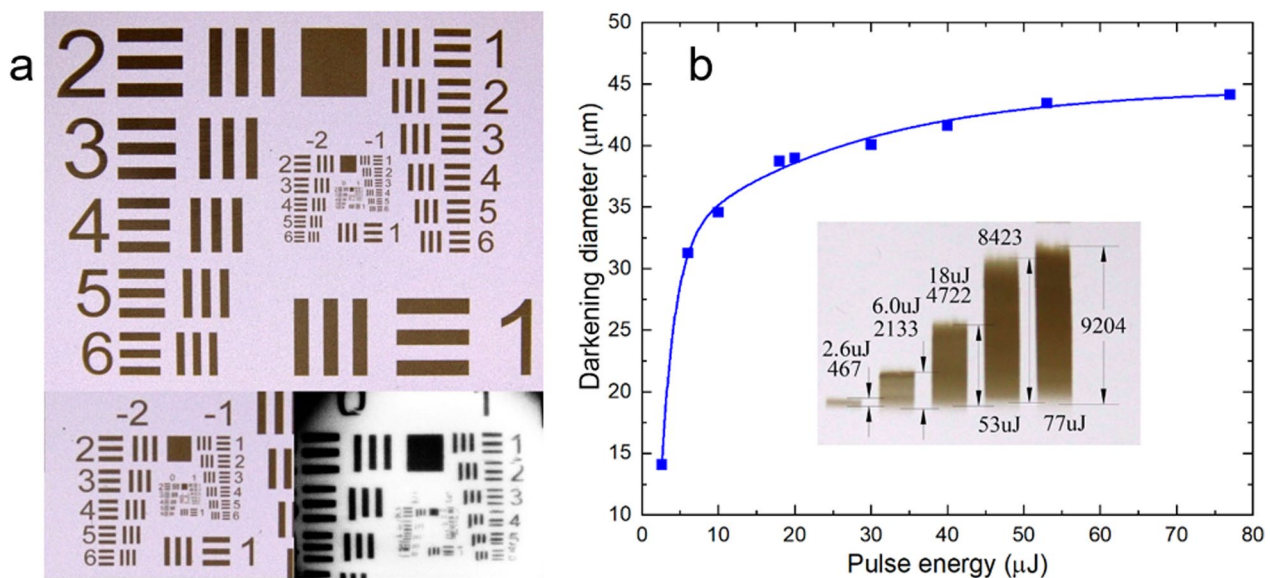
Fig. 11 a A standard 1951 USAF resolution test chart showing successively enlarged sections. First group has a period of about 1440 µm, while for the last group in the center, the period is ~ 7 µm. **b** Calculated diameter of the area with laser intensity above the darken-ing threshold depending on pulse energy. Insert: heights of modified regions depending on pulse energy. The photo was taken from the side (perpendicular to the laser beam propagation direction)

product of the pulse energy and the total number of pulses per unit area. The calculated values of the diameter of the area with laser intensity above the darkening threshold as a function of pulse energy are shown in Fig. 11b.

During laser processing, filamentation in the volume of glass and supercontinuum were observed with the naked eye. In the rough approximation described above, filamentation was not taken into account. It should serve only as an upper estimate for the colored track diameter based on the experimentally measured heights of the modified regions.

The track diameters depending on the pulse energy were also measured experimentally. Since a single track was too transparent to measure its diameter, lines 10 mm long were written in a thick sample and their transverse dimensions were measured. The pulse energies used were 2.5, 10, 20, 30, 40, and 100 µJ and scanning speed was 5 mm/s. The measured diameters of the thin sections of the tracks turned out to be approximately 6 µm for 2.5 µJ and 20–25 µm for higher energies, respectively.

As a demonstration of one possible application, a black and white image was written into glass (Sample 3) using the galvo scanner software. The original image (Fig. 12a) was generated by artificial intelligence and was written in three different modes. In the first mode (Fig. 12b), the image was divided into 20 layers, each containing a portion of the image with a certain grayscale range of 0–255. The grayscale range for the first layer was 30–40, and for the last layer 30–230, the step between layers was 10. Thus, the laser beam scanned the darker areas of the image more times, which caused stronger generation of color centers and darkening. In addition, to achieve a higher definition of the written image, different scanning speeds were set for the layers. The laser beam passed through the dark areas of the image more slowly, and through the light ones faster. The pulse energy used was 40 µJ and scanning speeds were 50 and 150 mm/s. In the central part of the image (at its edges) imperfections are visible, caused by the transition from one layer to another. The size of written image is 50×50 mm^2.

In the second mode (Fig. 12c), the image was pre-processed with Floyd–Steinberg dithering and then split into 16 layers with the grayscale step of 15. Despite the smaller number of layers, the written image contained fewer imperfections but had additional noise due to dithering.

In the third mode (Fig. 12d), the image was divided into 51 layers with a grayscale range of 0–5 for the first layer and 0–255 for the last layer, with a step of 5 between layers. The best image quality was achieved, but at the cost of increased processing time (115 min).

These results demonstrate the potential for achieving even higher writing quality through careful tuning of parameters such as number of layers, scanning speed, and pulse energy.

5 Conclusion

The investigation of the darkening effect of femtosecond infrared radiation on soda-lime glass is an area of interest for both scientific and practical purposes. This article

Fig. 12 a The original image. **b** The photo of an image, written in glass (Sample 3). 20 grayscale layers were used. **c** 16 grayscale layers and image pre-processing by Floyd–Steinberg dithering. **d** 51 grayscale layers

demonstrates that darkening effect can be utilized for the creation of halftone monochrome images for decorative purposes. However, limited optical density and thermal stability currently hinder the widespread implementation of this technology in industry. The factors influencing the kinetics of bleaching and the temporal stability of various types of glasses remain unclear, necessitating further research. It is also necessary to investigate whether it is possible to achieve different colors.

Regarding the process of monochrome images writing, the following conclusions can be drawn. The optical density magnitude of the modified regions depends on the exposure to laser radiation and is additive. Moreover, there are a lower limit and upper limit (saturated) concentrations of color centers, which are determined by the properties of the glass used. During laser processing, the color centers concentration asymptotically tends to its upper limit value. A nonzero lower limit concentration of color centers during relaxation is also observed.

The glass used for writing can be characterized by a set of constants: C_0, C_s, k, β, ζ, and χ, while the first two can be directly measured in the experiment. For writing, the knowledge of the first four (C_0, C_s, k, β) is required. The

description of relaxation additionally requires ζ and χ. The relaxation of color centers strongly depends on temperature and, for a specific glass, can be characterized by a constant χ.

The observed changes in the refractive index are slight, weakly dependent on the exposure, and, on the contrary, strongly depend on the pulse energy.

The glass (sample 3) used in our experiments on writing monochrome images is characterized by optical latitude $L_3 \sim 1$ and contrast $\gamma_3 \sim 0.22$. Since optical density is directly proportional to sample thickness, contrast in theory can be improved using thicker samples. However, the contrast value decreases with time due to color centers relaxation.

The resolution of the written test chart, which was achieved using a conventional commercial galvo scanner with an F-theta lens, is $\sim 10\mu m$. High resolution and the use of well-known dithering methods make it possible to obtain a continuous gray scale.

The technology presented in this study has the potential for use in the semiconductor and photonic industries, where it could lead to new opportunities in the high-tech device development. High-resolution three-dimensional patterns created in glass possess a spatially non-uniform impedance

distribution for low-frequency electric fields ($10^4 \div 10^6$ Hz). These elements are in high demand [19, 20] for the production of advanced phase LCD devices, including deflectors and lenses, among others.

Declarations

Conflict of interest The authors declare that they have no conflict of interest.

References

1. R. Stoian, Appl. Phys. A **126**, 438 (2020). https://doi.org/10.1007/s00339-020-03516-3
2. M. Sakakura, Y. Lei, L. Wang, Y.-H. Yu, P.G. Kazansky, Light Sci Appl **9**, 15 (2020). https://doi.org/10.1038/s41377-020-0250-y
3. C. Vetter, R. Giust, L. Furfaro, C. Billet, L. Froehly, F. Courvoisier, Materials **14**, 6749 (2021). https://doi.org/10.3390/ma14226749
4. J.B. Lonzaga, S.M. Avanesyan, S.C. Langford, J.T. Dickinson, J. Appl. Phys. **94**, 4332 (2003). https://doi.org/10.1063/1.1603962
5. J.T. Dickinson, S. Orlando, S.M. Avanesyan, S.C. Langford, Appl. Phys. A **79**, 859 (2004). https://doi.org/10.1007/s00339-004-2571-8
6. D. Ashkenasi, A. Lemke, J. Laser Appl. **23**, 012007 (2011). https://doi.org/10.2351/1.3558996
7. A. Bishay, J. Non-Cryst. Solids **3**, 54 (1970)
8. D. L. Griscom, in *Radiation Effects on Optical Materials* (SPIE, 1985), pp. 38–59.
9. J. Sheng, K. Kadono, T. Yazawa, Appl. Radiat. Isot. **57**, 813 (2002). https://doi.org/10.1016/S0969-8043(02)00232-4
10. J. Sheng, X. Yang, W. Dong, J. Zhang, Int. J. Hydrogen Energy **34**, 3988 (2009). https://doi.org/10.1016/j.ijhydene.2009.03.021
11. K. Kadono, N. Itakura, T. Akai, M. Yamashita, T. Yazawa, Nucl. Instrum. Methods Phys. Res., Sect. B **267**, 2411 (2009). https://doi.org/10.1016/j.nimb.2009.04.014
12. A. Serrano, F. Gálvez, O. Rodríguez de la Fuente, M.A. García, J. Appl. Phys. **113**, 113104 (2013). https://doi.org/10.1063/1.4794807
13. K. Kadono, N. Itakura, T. Akai, M. Yamashita, T. Yazawa, J. Phys. Condens. Matter **22**, 045901 (2010). https://doi.org/10.1088/0953-8984/22/4/045901
14. J. Sheng, Y. Wu, X. Yang, J. Zhang, Int. J. Hydrogen Energy **34**, 1123 (2009). https://doi.org/10.1016/j.ijhydene.2008.10.097
15. M. Born and E. Wolf, *Principles of Optics: Electromagnetic Theory of Propagation, Interference and Diffraction of Light*, 7th ed. (Cambridge University Press, Cambridge, 1999). https://doi.org/10.1017/CBO9781139644181
16. D.L. Griscom, Phys. Rev. B **64**, 174201 (2001). https://doi.org/10.1103/PhysRevB.64.174201
17. V. A. Mashkov, Wm. R. Austin, L. Zhang, and R. G. Leisure, Phys. Rev. Lett. **76**, 2926 (1996). https://doi.org/10.1103/PhysRevLett.76.2926
18. M. Rubin, Solar Energy Mater. **12**, 275 (1985)
19. M. Ye, B. Wang, and S. Sato, Opt. Express, OE **16**, 4302 (2008). https://doi.org/10.1364/OE.16.004302
20. O. Sova, V. Reshetnyak, T. Galstian, and K. Asatryan, J. Opt. Soc. Am. A, JOSAA **32**, 803 (2015). https://doi.org/10.1364/JOSAA.32.000803